On Spectral Analysis of Mesoscale Eddies. Part II: Nonlinear Analysis

P. BERLOFF

Department of Mathematics, and Grantham Institute for Climate Change, Imperial College London, London, United Kingdom

I. KAMENKOVICH

Rosenstiel School of Marine and Atmospheric Science, University of Miami, Miami, Florida

(Manuscript received 30 November 2012, in final form 3 September 2013)

ABSTRACT

Several turbulent flow regimes of an idealized ocean circulation model are systematically analyzed in physical and spectral domains. Zonal dispersion properties of transient mesoscale eddies are described by the zonal wavenumber/temporal frequency spectra. The eddy patterns and the corresponding nonlinear eddy forcing exerted on the jets are examined by filtering different parts of the spectra. Comparison of the outcome of this nonlinear analysis with the properties of the linearized solutions (obtained in Part I of this paper) demonstrates that a very substantial part of the flow dynamics is controlled by the underlying linear dynamics. This result supports the hypothesis that it is possible to describe most of the oceanic mesoscale eddies as a wave turbulence phenomenon.

1. Motivations and main goals

The main goal of this paper is to make progress in understanding to what extent and how properties of eddies are controlled by underlying linear dynamics. In Part I of this paper [Berloff and Kamenkovich (2013), hereafter Part I; section 1a], we explain why understanding the linear control is an important and controversial subject, provide the relevant background, describe the numerical simulations characterized by emergence of stationary alternating multiple zonal jets, and systematically analyze the linear-dynamics properties of a hierarchy of background flows, from horizontally uniform to those that include the jets. The outcome of the linear analysis is in terms of a spectrum of the linear normal modes, which are characterized by their dispersion relationships, horizontal patterns, vertical structures, correlations with the multiple jets, and by their nonlinear self-interactions projecting on the jets. This paper focuses on the spectral properties of the fully nonlinear solutions from the numerical simulations described in Part I. These properties are compared with those of the linear solutions of Part I, helping to assess the degree of the linear control. We also discuss such purely nonlinear characteristics as the spectral energetics and properties of isolated coherent eddies.

The plan of the paper is the following. In section 2, we discuss such properties of the eddies as their energetics and wavenumber/frequency spectra. Section 3 deals with distinct classes and properties of the eddies spectrally filtered from the zonal wavenumber/frequency spectra. Comparison of the nonlinear eddies and the underlying linear normal modes leads us to important conclusions about the degree of the linear control (section 4).

2. General properties of the nonlinear eddies: Energetics and spectra

We consider several distinct flow regimes characterized by different background flows (i.e., eastward- and westward-background flows: EB and WB regimes, respectively), intermediate and large Reynolds numbers Re, and the three values of the bottom friction coefficient γ, which controls latency of the alternating jets (see Table 1 and Fig. 1 in Part I). This section deals with the energetics of the flow and the general properties of the eddy k–ω spectra, where k is zonal wavenumber, and

Corresponding author address: P. Berloff, Department of Mathematics, Imperial College London, Huxley Bldg., London, SW7 2AZ, United Kingdom.
E-mail: p.berloff@ic.ac.uk

DOI: 10.1175/JPO-D-12-0233.1

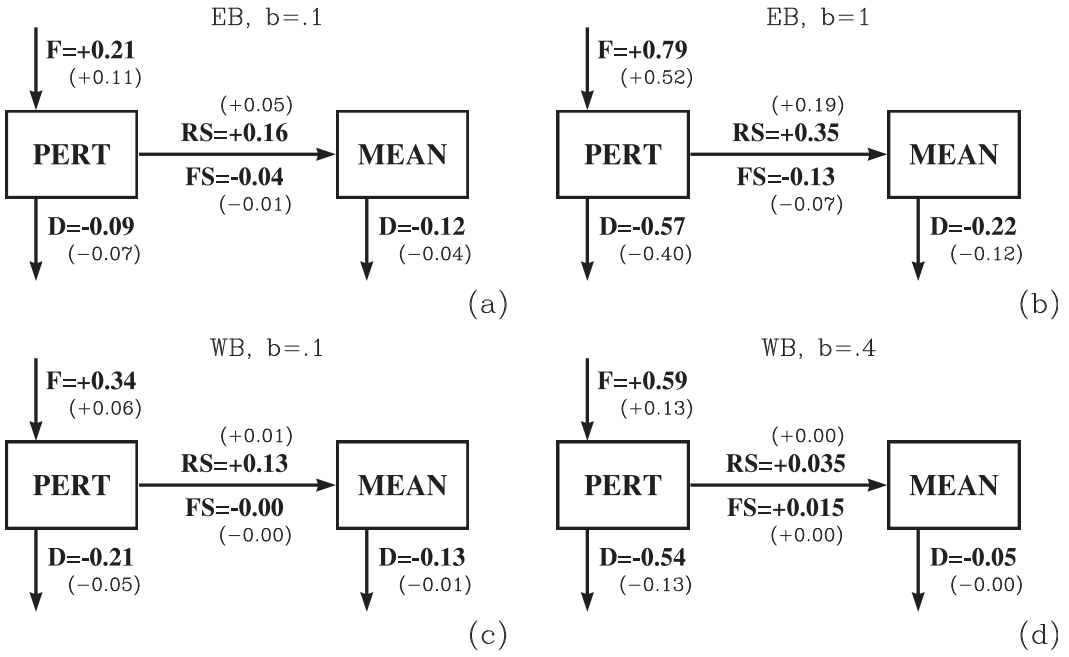

FIG. 1. Schematic diagrams of the energetics. Shown are the energetic balances for the bottom friction values of (a) 10^{-8}, (b) 10^{-7}, (c) 10^{-8}, and (d) $0.4 \times 10^{-7}\,\mathrm{s}^{-1}$ for (top) the EB- and (bottom) WB-flow regimes. Perturbations and mean flow are indicated by the corresponding rectangles; F is forcing, D is dissipation, and the energy exchange terms due to the Reynolds and form stresses are denoted by RS and FS, respectively. Boldface values correspond to the large-Re solutions, and values in the brackets correspond to the moderate-Re solutions. All values are normalized by the energy of fluctuations.

ω is time frequency. We also quantify spectral contribution of the isolated, intense coherent vortices emerging in the large-Re flow regimes.

a. Energetics

Flow energetics is a useful starting point, as it provides compact information characterizing the flow. Basic energetics of the flow (minus the constant background flow) is expressed in terms of the basin- (over area A of the domain) and time-averaged (denoted by overbar) total energy E, internal "forcing" (i.e., baroclinic energy transfer from the large-scale background flow state) F, and energy dissipation D:

$$E = \frac{1}{A}\int\int_A \left[\sum_{i=1,2}\frac{H_i}{H}\frac{\overline{(\nabla\psi_i)^2}}{2} + \frac{S_1H_1 + S_2H_2}{4H}\overline{(\psi_1-\psi_2)^2}\right] dx\,dy, \tag{1}$$

$$F = -\frac{U}{A}\frac{H_1}{H}\int\int_A \overline{\psi_1\frac{\partial\zeta_1}{\partial x}}\,dx\,dy, \quad \text{and} \tag{2}$$

$$D = -\frac{1}{A}\int\int_A \left[\nu\sum_{i=1,2}\frac{H_i}{H}\overline{(\nabla^2\psi_i)^2} + \gamma\frac{H_2}{H}\overline{(\nabla\psi_2)^2}\right] dx\,dy. \tag{3}$$

We decompose the flow into the zonally uniform time-mean jets $u_i(y)$ and fluctuations around them. Then, E is split into the time-mean and fluctuation energies, F acts only on the fluctuations, and D is split into the time-mean and fluctuation dissipations. The time-mean flow is forced by the energy conversion terms, E_{RS} and E_{FS}, which transfer energy because of the work done by horizontal Reynolds stresses and by isopycnal form stress, respectively:

$$E_{\mathrm{RS}} = \sum_{i=1,2}\frac{H_i}{H}\frac{\partial\psi_1'}{\partial y}\frac{\partial\psi_1'}{\partial x}\frac{\partial\overline{u}_1}{\partial y} \quad \text{and}$$

$$E_{\mathrm{FS}} = \frac{S_1H_1 + S_2H_2}{2H}(\psi_1' - \psi_2')\frac{\partial(\psi_1' + \psi_2')}{\partial x}(\overline{u}_1 - \overline{u}_2). \tag{4}$$

Basic energetics of the flow (Fig. 1) gives a useful description of the flow dynamics in the presence of jets. First, by relating F and D to the total fluctuation energy, we find that the system is strongly forced and damped, and even more so when γ is not small and the jets are more latent. At a moderate Re the basic energetics are qualitatively similar, but significantly less forced and dissipative (relative to the energy of the eddies), particularly in the WB-flow regimes. Second, the energy

conversion is dominated by E_{RS}, and this energy conversion term is always directed from the eddies toward the time-mean flow (i.e., ''negative viscosity'' effect). The form stress energy conversion term E_{FS} can have either sign. In the EB-flow regimes, it is negative, that is, the time-mean flow returns some energy to the eddies through the baroclinic instability mechanism. In the WB-flow regimes, E_{FS} is negligible for weak bottom friction, but otherwise it is positive, indicating that the eddies on average maintain the jets by diverging eddy buoyancy fluxes. Note that, although it is possible to calculate contributions of each individual normal mode into these energy conversion terms, the net E_{FS} and E_{RS} terms are simply not available from the linear problem and cannot be compared to these results. Our energy conversion results are broadly consistent with findings of Berloff et al. (2009), and the energetics focusing on different eddy classes is discussed further below, in section 3.

b. *Spectra of the eddies*

Now, we turn our attention to spectral properties of the flow solutions. Our approach is to focus on the k–ω spectra, and we argue that these spectra are particularly useful in this study, because not only they contain information on the zonal propagation of eddies, but also they are more efficient in describing eddies localized on individual east- or westward jets rather than homogeneously distributed in space. Even more useful will be projection of the eddies on the linear normal modes, but this extension is beyond the scope of this paper. In the previous studies of anisotropic geostrophic turbulence attention was paid mostly to wavenumber spectrum: either two-dimensional k–l spectrum (e.g., Vallis and Maltrud 1993), where l stands for the meridional wavenumber, or isotropic wavenumber spectrum (e.g., Galperin et al. 2010). One-dimensional frequency spectrum (typically measured by current meters mounted on ocean moorings) is also used for characterizing oceanic eddies. These more conventional spectra are described in the appendix, where the connection to the k–ω spectra is also made.

The k–ω spectra were calculated by the two-dimensional Fourier transform in longitude and time of the velocity streamfunction anomaly and for each isopycnal layer. After removing the zonal time mean from the record, it was tapered to zero in time by a Tukey (or tapered cosine) window that decreases smoothly from unity to zero over 20 temporal grid points. Each latitude was treated independently, and the outcome was averaged over the latitudes to yield the final spectrum. When the frequency is negative, we trade its sign for the negative sign of k; thus, Fourier modes with negative/positive k have west-/eastward phase speeds.

We examined 12 flow solutions corresponding to different dynamical regimes: for a moderate and large Reynolds number, for eastward- and westward-background flow regimes, and for three different values of the bottom friction coefficient (more details of the solutions are in Part I). Different background flows result in dynamically very different regimes; different bottom friction coefficients produce strong (nonlatent) jets, moderate (latent) jets, and no stationary jets; and different Re allow to look at different levels of the nonlinearity. The resulting nonlinear k–ω spectra are shown for moderate-Re EB- (Fig. 2), moderate-Re WB- (Fig. 3), large-Re EB- (Fig. 4), and large-Re WB-flow regimes (Fig. 5). These spectra can be compared with the linear ensemble-averaged spectra of Part I (Figs. 9–12 of Part I), under the standard assumption, that the most unstable normal modes in the linear problem can be expected to dominate the nonlinear spectrum. As we show below, this assumption is not accurate in many cases, indicating an importance of modes that do not have unstable growth rates. For each nonlinear solution, we focus on different spectral regions, outlined by sets of quadrangles in the plots, and for the upcoming analysis spectrally filter out the eddies corresponding to each quadrangle.

There are two groups of quadrangles. The first group corresponds to spectral regions of positive linear growth rates and is adopted from Part I (Figs. 9–12 in Part I). We refer to the eddies from these quadrangles as westward mesoscale eddies (WME) or eastward mesoscale eddies (EME), depending on whether they correspond to negative or positive k in the k–ω spectrum, respectively. Examples of WME and EME quadrangles are numbered 1 and 2, respectively, in Fig. 4a. The second group of quadrangles outlines parts of the spectra that do not correspond to strong growth in the linear problem, but correspond to large spectral power in the nonlinear regime. Examples of those modes include slow meander eddies (SME), as indicated by quadrangles 3a and 3b in Fig. 4a—these are mesoscale eddies that form strong meanders on the eastward jets (as shown further below). Another type of eddies, high-frequency basin modes (HFBM), are indicated, for example, by quadrangle 4 in Fig. 4a—the larger the γ, the less power is contained in these modes. We argue that this is because of the strong damping of the underlying linear normal modes; see Part I. Another type of eddies, large-scale low-frequency modes (LSLFM), are defined as flow features from near the origin of k–ω spectrum (e.g., quadrangle 6 in Fig. 4a). The spectral power of LSLFM is larger for larger Re, indicating more vigorous energy transfers from smaller to larger scales. Alternating zonal jets, which correspond to $k = 0$, can be interpreted as the extreme LSLFM patterns, and they also get stronger for larger Re. The last type of

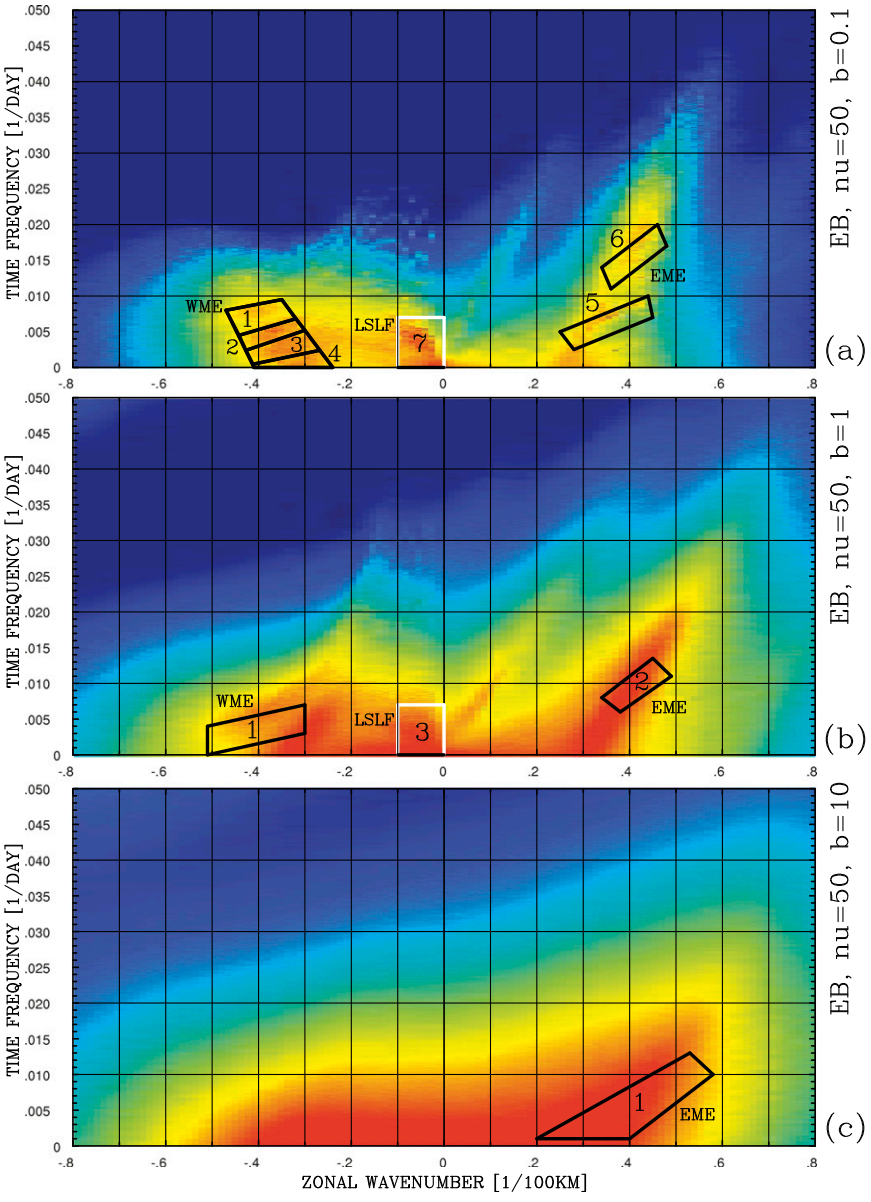

FIG. 2. Spectrum of the nonlinear reference solution: EB-flow case with a moderate Re. This figure is to be compared with Fig. 9 in Part I. Plotted is $\log_{10}$ of the power, and the color scale is the same for all panels. Black quadrangles correspond to the normal modes with the most unstable growth rates, and white quadrangles correspond to other spectral regions with significant power. Panels correspond to three different values of bottom friction γ: (a) 10^{-8}, (b) 10^{-7}, and (c) $10^{-6}\,\mathrm{s}^{-1}$.

eddies, fast eastward modes (FEM), (e.g., quadrangle 5 in Fig. 4a) populate the part of the spectrum corresponding to the fastest eastward-propagating nondispersive normal modes.

Deep-ocean k–ω spectra (not shown) are qualitatively similar to the upper-ocean ones but have less power, because eddies are weaker in the deep layer. The only exception is the westward-propagating high-frequency eddies, which resemble the underlying and mostly barotropic normal modes. Below, we focus our presentation on the upper-ocean spectra, but all of our analyses consider both layers.

In the large-Re solutions, particularly in the WB-flow regimes, there are numerous long-lived isolated coherent vortices (corresponding to the extreme-value anomalies in Fig. 1 of Part I), which are strongly nonlinear features with no resemblance of the underlying linear normal modes. A systematic and detailed study of these vortices

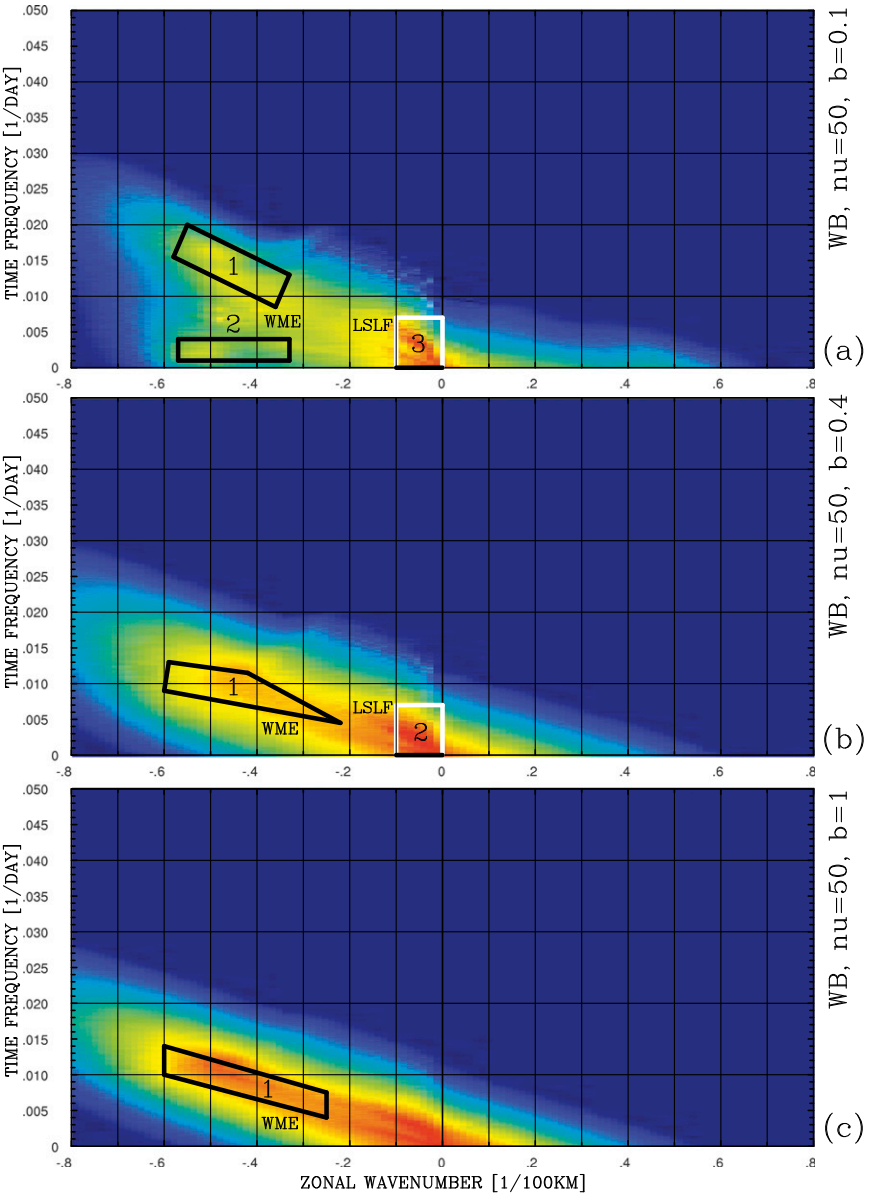

FIG. 3. Spectrum of the nonlinear reference solution: WB-flow case with a moderate Re. This figure is to be compared with Fig. 10 in Part I. The outline is similar to Fig. 2. Panels correspond to three different values of bottom friction γ: (a) 10^{-8}, (b) 4×10^{-8}, and (c) 10^{-7} s^{-1}.

deserves a separate study, but here we mention several relevant and important points. First, we estimated contributions of the vortices to the k–ω spectra, and the outcome is shown in Fig. 6 for the WB-flow regime, characterized by the most pronounced vortex population. Because these vortices correspond to very large amplitudes, we defined them in the most straightforward way by cutting off the large-amplitude anomalies of the velocity streamfunction at a certain value. We checked that the outcome is qualitatively insensitive to a reasonable range of the streamfunction cutoff levels. Thus, we statistically decomposed the flow into the ''high passed'' and ''low passed'' components representing the vortices and the rest of the eddies, respectively. We found that the imprint of these vortices on to the spectrum is in the form of the nearly nondispersive tongue of mostly westward-propagating flow anomalies. This is similar to the situation when strong vortex nonlinearity couples the normal modes and prevents their dispersion (e.g., Early et al. 2011). In the EB-flow regime, characterized by fewer, less-intense, and shorter-lived vortices, contribution of these vortices to the k–ω spectrum is small

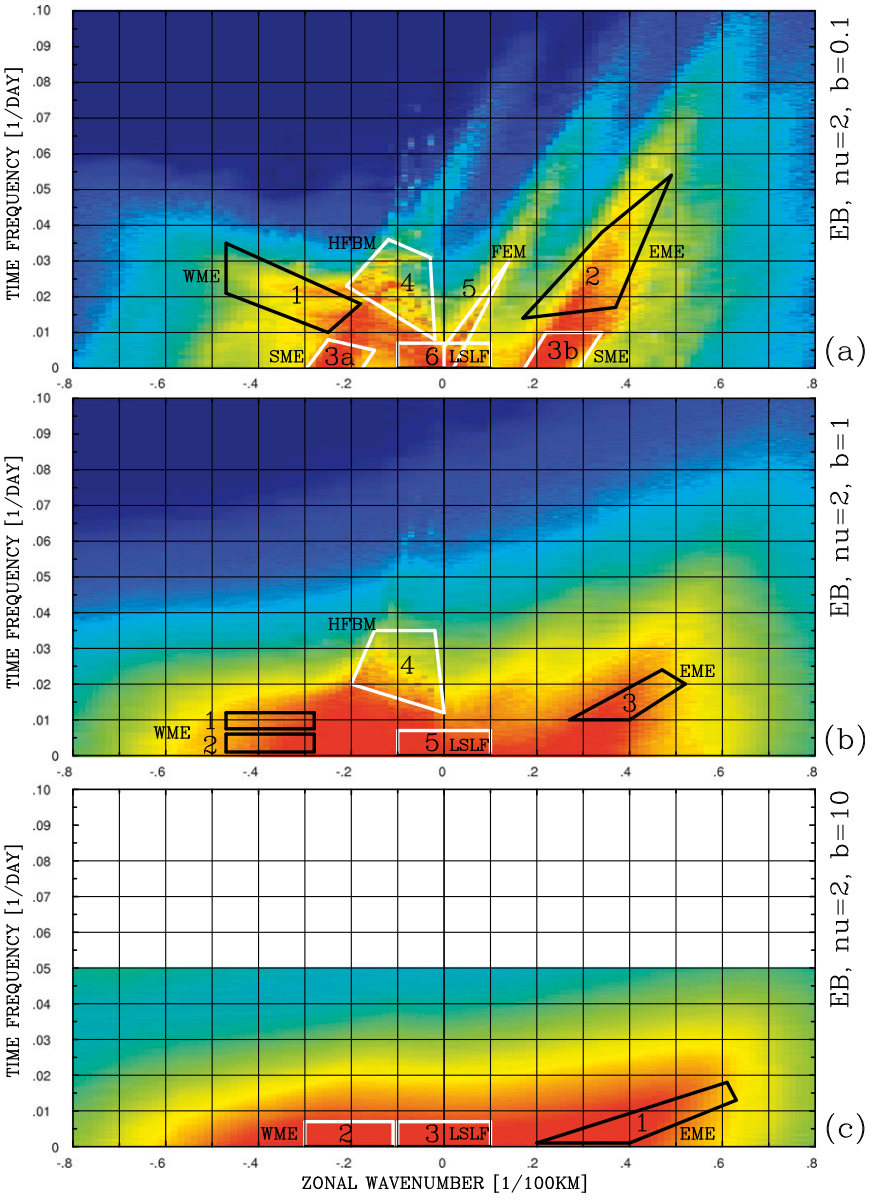

FIG. 4. Spectrum of the nonlinear reference solution: EB-flow case with a large Re. This figure is to be compared with Fig. 11 in Part I. The outline is similar to Fig. 2. Panels correspond to three different values of bottom friction γ: (a) 10^{-8}, (b) 10^{-7}, and (c) 10^{-6} s^{-1}.

and insignificant. To summarize, the spectral contribution of the isolated coherent vortices is relatively small; and the focus of our study is on the remaining part of the flow.

We also looked at the energetics of the vortices by treating them as fluctuations on the top of the time-mean flow (see section 2a). This exercise suggested that in the WB-flow regime the vortices are energized directly and substantially by the baroclinic instability of the uniform background flow, whereas in the EB-flow regime the vortices are instead weakly forced by the mixed baroclinic and barotropic instabilities of the jets rather than by baroclinic instability of the uniform background flow. Thus, at least in one flow regime dynamical understanding of the vortices may require consideration of the jets, but detailed dynamical analysis of the jet/vortices interactions is also beyond the scope of this paper.

3. Analysis of k–ω spectra

This section deals with analyses of distinct classes of eddies filtered from the k–ω spectra and their properties, such as structure, energetics, and eddy forcing exerted

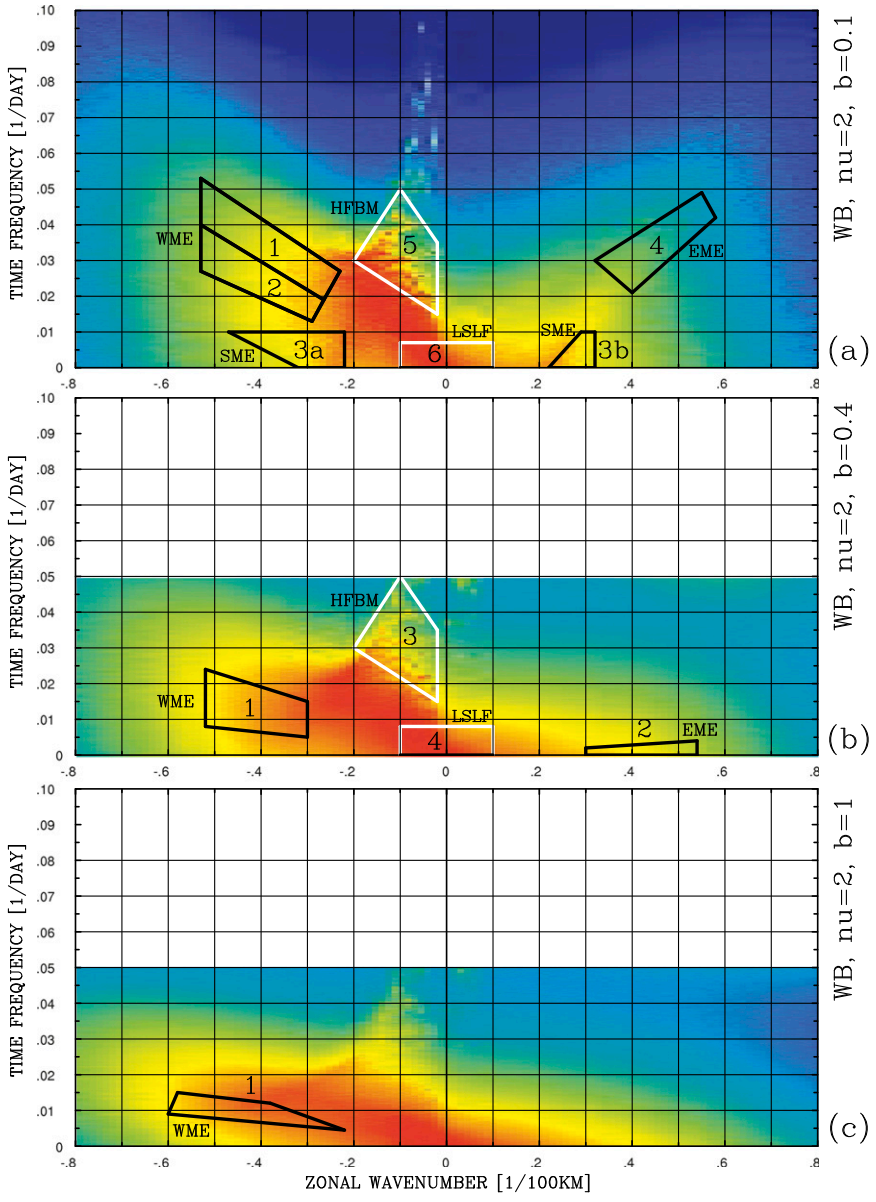

FIG. 5. Spectrum of the nonlinear reference solution: WB-flow case with a large Re. This figure is to be compared with Fig. 12 in Part I. The outline is similar to Fig. 2. Panels correspond to three different values of bottom friction γ: (a) 10^{-8}, (b) 4×10^{-8}, and (c) 10^{-7} s^{-1}.

on the underlying jets. First, in each layer we examined the patterns of the eddies (Fig. 7) and correlated the meridional profiles of the corresponding zonally and temporally averaged eddy kinetic energies with the meridional profiles of zonal velocity of the underlying jets. This calculation can tell whether the eddies straddle preferentially west- or eastward jets, or both of them equally. Second, to understand how the eddies interact with the underlying jets, we calculated correlations of the corresponding eddy forcing and its components with the potential vorticity (PV) anomalies associated with the jets. Note that because the jets are affected only by self-interactions of each spectral mode, contributions of all individual modes to the eddy forcing are additive. Finally, we calculated meridional correlations of the eddies, in order to estimate the degree of their meridional localization on the jets. The above analyses are then compared with the corresponding properties of the underlying linear normal modes (Part I).

a. General properties of the nonlinear eddies

Some flow patterns corresponding to the WME, EME, SME, HFBM, FEM, and LSLFM eddy classes

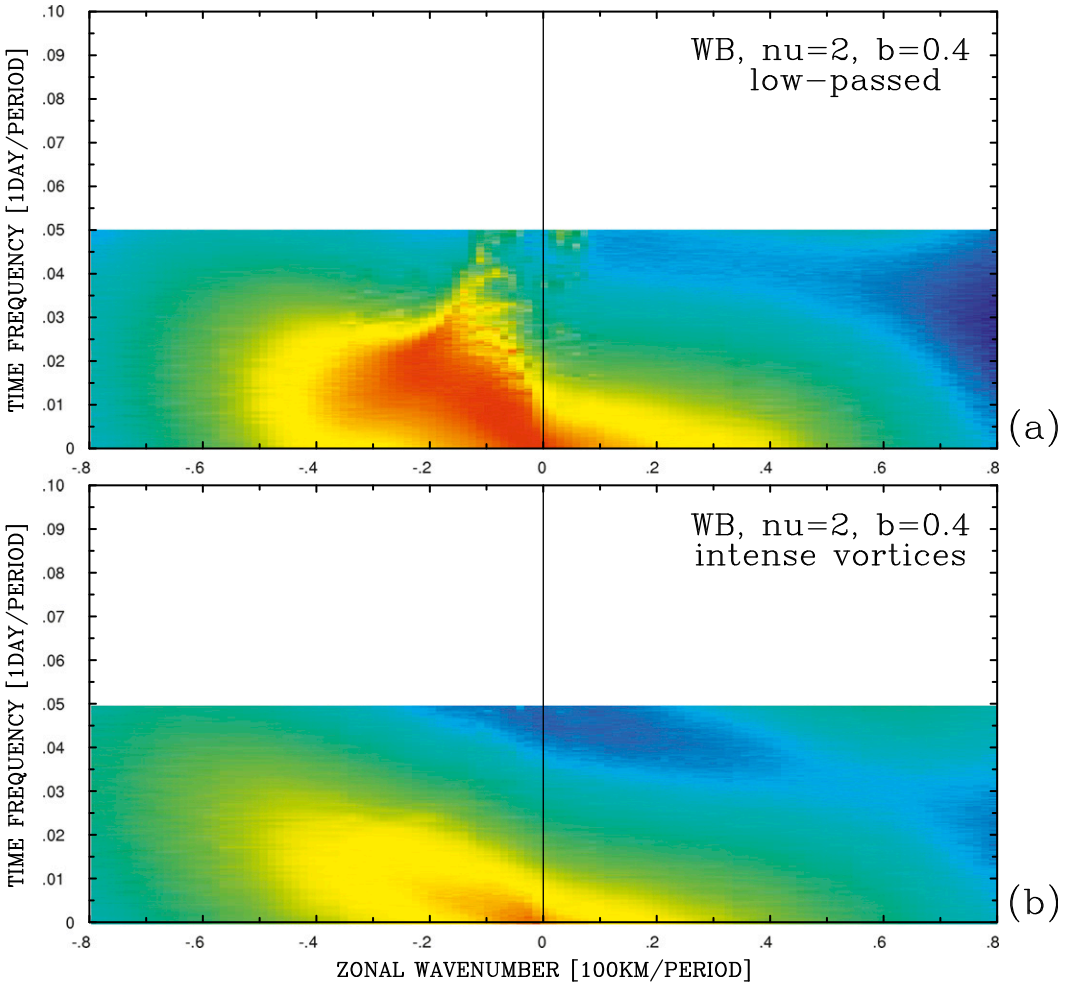

FIG. 6. Contribution of intense long-lived vortices to the spectrum. Decomposition of the nonlinear reference solution in the WB-flow case with a large Re and medium bottom friction (Fig. 5b) into (a) the low-passed and (b) intense-vortex parts of the flow. Note that vortices do not project on the higher-frequency baroclinic modes. In the EB solutions, the low-passed and intense-vortex spectra are qualitatively similar.

(outlined by the quadrangles in the spectra) are illustrated in Fig. 7. Visual inspection of the EME and WME spatial structures suggests that they are very similar to the underlying normal modes [not shown here, but see Berloff et al. (2009) for their details], and more so in the moderate-Re case. The HFBM eddies seem to be the least affected by the jets; the FEM eddies can be characterized as large-scale zonal velocity anomalies localized on the cores of the eastward jets; and the LSLF eddies can be interpreted as either transient zonal jets or low-frequency variability of the underlying jets.[1] Finally, the SME patterns consist of large-amplitude slowly propagating meanders, which are strongly correlated with the jets. Further below we argue that all of the above patterns, except for SME, look similar to the underlying normal modes.

We analyzed vertical structures of the filtered eddy classes by calculating (i) ratios between the standard deviations of the instantaneous barotropic and baroclinic mode amplitudes and (ii) correlations between the barotropic and baroclinic modes. These measures are analogous to the normal-mode vertical mixing and coupling discussed in Part I, and the outcome is broadly consistent with the linear-analysis predictions. Ratio of the barotropic-to-baroclinic mode amplitude is mostly about unity, suggesting that no parts of the spectra are occupied by predominantly barotropic or baroclinic

[1] It is argued that these zonally extended modes are the main contributors to zonal eddy-induced material transport (I. Kamenovich et al. 2013, unpublished manuscript).

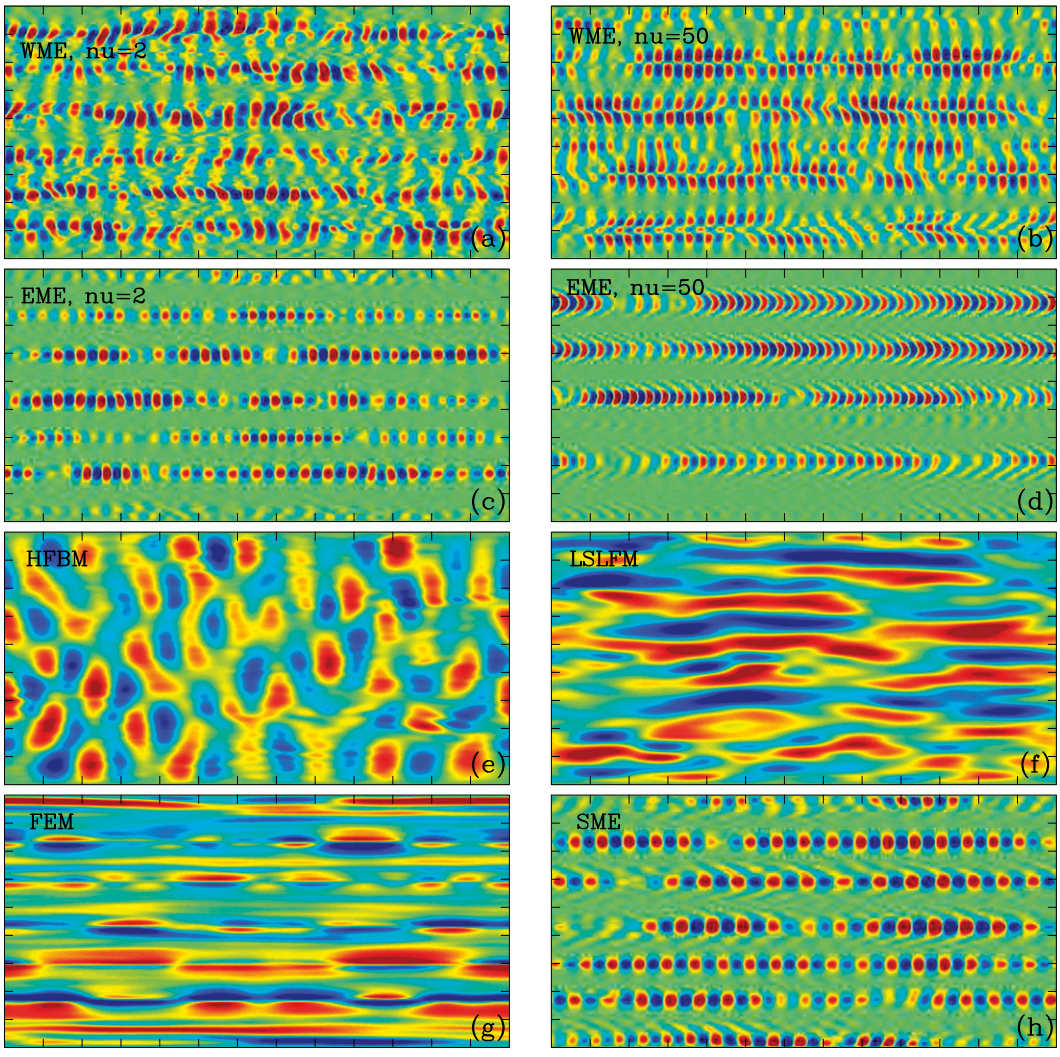

FIG. 7. Different types of eddies: snapshots of k–ω spectrally filtered flow fluctuations. Patterns of the upper-ocean velocity streamfunctions are shown (arbitrary units). (a) WME with a large Re (box 1 from Fig. 4a); (b) WME with a moderate Re (box 2 from Fig. 2a); (c) EME with a large Re (box 2 from Fig. 4a); (d) EME with a moderate Re (box 6 from Fig. 2a); (e) HFBM (box 5 from Fig. 5a); (f) LSLFM (box 4 from Fig. 5b); (g) FEM (box 5 from Fig. 4a); and (h) SME (box 3b from Fig. 4a).

modes. The only part of the spectrum where this ratio is relatively large (about 3–6) corresponds to HFBM eddies and indicates that they are predominantly barotropic. Correlations between the barotropic and baroclinic vertical modes are not only significant but also tend to have the sign predicted by the linear analysis. In the EB-flow regime, correlation between the modes varies from 0.5 to 0.9 (surface intensified). In the WB-flow regime, it varies from -0.6 (bottom intensified) to 0.2.

From visual comparison of the nonlinear and the linear ensemble-averaged spectra, we identified the following similarities. First, there is a large overlap between the parts of each spectrum containing significant power and the k–ω regions populated by the linear normal modes, suggesting that fluctuations are weak, if they cannot project on the underlying normal modes. Second, most of the nonlinear spectral power occupies regions of the nearly neutral (or, weakly damped) linear modes (green regions in the linear ensemble-averaged spectra: Figs. 9–12 in Part I). Most of these regions have $|k|$ smaller than those of the most unstable mesoscale modes. It is, therefore, very likely that the corresponding scales are excited by upscale energy transfers associated with nonlinear interactions. Third, some of the linear dispersion curves or clusters of curves (e.g., corresponding to HFBM eddies), are visible in the nonlinear spectra, augmenting the idea of the underlying linear control. Finally, further below we analyze patterns

TABLE 1. Energetics of large-Re eddies filtered in the k–ω spectral domain. Left column indicates quadrangles, and the other columns correspond to the EB- and WB-flow regimes with weak and medium values of the bottom friction coefficient. In each box of the table: the first line contains abbreviation used for eddies in this region of spectrum. Units of E are $10^{-4}\,m^2\,s^{-2}$; F and D are normalized by the corresponding value of E. Thus, the corresponding values can be interpreted as the forcing and dissipation efficiencies.

	EB, $\gamma = 0.1$				EB, $\gamma = 1$			
		E	F	D		E	F	D
1	WME	0.42	0.159	−0.005	WME	0.49	0.083	−0.019
2	EME	1.44	0.100	−0.005	SME	0.50	0.086	−0.019
3	—	—	—	—	EME	1.96	0.220	−0.020
3a	SME	2.45	0.013	−0.007	—	—	—	—
3b	SME	4.24	0.031	−0.006	—	—	—	—
4	HFBM	0.31	0.004	−0.007	HFBM	0.40	0.035	−0.038
5	FEM	0.85	0.008	−0.008	LSLFM	3.31	0.013	−0.028
6	LSLFM	0.78	0.005	−0.007	—	—	—	—
	WB, $\gamma = 0.1$				WB, $\gamma = 0.4$			
1	WME	0.79	0.125	−0.011	WME	2.03	0.137	−0.028
2	WME	0.59	0.128	−0.011	EME	0.25	0.168	−0.028
3	—	—	—	—	HFBM	0.29	−0.014	−0.026
3a	SME	0.66	0.137	−0.011	—	—	—	—
3b	SME	0.32	0.120	−0.013	—	—	—	—
4	EME	0.20	0.170	−0.017	LSLFM	6.18	0.016	−0.028
5	HFBM	0.87	0.006	−0.009	—	—	—	—
6	LSLFM	4.15	0.012	−0.009	—	—	—	—

TABLE 2. Energetics of moderate-Re eddies filtered in the k–ω spectral domain. Layout and notations are as in Table 1.

	EB, $\gamma = 0.1$				EB, $\gamma = 1$			
		E	F	D		E	F	D
1	WME	0.09	0.170	−0.049	WME	0.37	0.181	−0.050
2	WME	0.12	0.171	−0.046	EME	1.29	0.252	−0.061
3	WME	0.16	0.183	−0.045	LSLFM	1.65	0.009	−0.042
4	Neither	0.09	0.162	−0.039	—	—	—	—
5	EME	0.13	0.253	−0.061	—	—	—	—
6	EME	0.12	0.366	−0.079	—	—	—	—
7	LSLFM	0.83	0.002	−0.029	—	—	—	—
	WB, $\gamma = 0.1$				WB, $\gamma = 0.4$			
1	WME	0.24	0.194	−0.071	WME	0.57	0.165	−0.075
2	EME	0.06	0.261	−0.101	LSLFM	0.65	0.014	−0.048
3	LSLFM	0.30	−0.007	−0.025	—	—	—	—

and eddy forcings of different eddy classes and find qualitative similarities with those of the corresponding linear normal modes.

There are, however, some substantial differences between the nonlinear and linear spectra. First, there is a tendency of the nonlinear spectral power to populate small-k and small-ω spectral region, and it is more pronounced at a large Re. In line with the previous studies of geostrophic turbulence, these results can mean that the eddy energy generated at mesoscales by flow instabilities, in the form of the most unstable normal modes, is channeled by nonlinear interactions to long zonal scales (small k) and low frequencies, where it eventually dissipates through the bottom friction. We leave analysis of the energy transfers between the normal modes for the future, but we note that this process can be very different from the classical ''inverse cascade'' conjecture that involves consecutive energy transfer between the neighboring Fourier modes, because in the presence of the jets the normal modes are not Fourier modes in meridional direction, and, therefore, ''neighboring'' them in the spectral space is ambiguous. Second, unstable regions in the linear spectra do not necessarily correspond to the spectral peaks in the corresponding nonlinear spectra. This is also consistent with the aforementioned idea of energy transfer from the growing mesoscales to long scales, where the energy accumulates. Third, some parts of the nonlinear spectra (e.g., SME) have no similarity with the underlying linear modes. Finally, strong coherent eddies—not controlled by the linear dynamics—are present in the large-Re solutions; their contribution to the k–ω spectra was discussed in section 2b.

b. *Analysis of different eddy classes*

We partially expanded analysis of the global energetics (section 2a) to characterize different regions of the k–ω spectra, by considering the total energy, forcing, and dissipation [defined in (1)–(3)] for each class of eddies (summarized in Tables 1 and 2). We left out analysis of the corresponding energy conversions because they involve nonlinear interactions with the fluctuations outside of the eddy classes (i.e., spectral quadrangles), whereas the focus of this paper is on interactions between the eddies and the jets. Several conclusions can be drawn from our analysis of the eddy energetics. First, energy tends to accumulate at large scales and low frequencies, and even more so at large Re. Second, all mesoscale parts of the spectra absorb more energy from the forcing than they release through the dissipation, and this is more so for the eddies corresponding to the most unstable underlying linear modes, such as WME and EME. This implies that the corresponding eddies transfer the excess of energy to other scales, including the larger scales, where more energy is dissipated than generated. At moderate Re the mesoscale energy forcing is larger, but so is the mesoscale dissipation. Therefore, the energy supply from the mesoscales is similar. Consistent with reduced viscosity, the dissipation at large Re is dominated by the bottom friction, whereas at moderate Re it is dominated by the

eddy viscosity, everywhere except for LSLFM eddies, where both dissipation processes have similar intensity. Third, forcing at large scales (small k) is weak, and at large/moderate Re it is weakly/strongly overtaken by the dissipation. The corresponding negative energy balance is consistent with the upscale energy transfer from the mesoscale WME and EME eddies. The above results prompt for an analysis of the classical triad interactions and the corresponding energy transfer between the normal modes, but this is beyond the scope of this paper.

To examine eddy feedbacks on the jets, the filtered eddies are used for calculating the corresponding eddy forcing F_i, and its Reynolds and form stress components (defined in section 2c, Part I). Note that only interactions of modes with the same k and ω can affect the stationary $k = 0$ jets, and therefore the eddy forcings of each of the eddy classes are additive. We also defined barotropic F_{BT} and baroclinic F_{BC} eddy forcings by projecting the governing equations on the vertical barotropic and baroclinic modes. For each spectral class, we calculated the zonal averages of the eddy forcing components and obtained the meridional profiles $F_{\mathrm{BT}}(\gamma)$ and $F_{\mathrm{BC}}(\gamma)$. $F_{\mathrm{BT}}(\gamma)$ is further separated into the two terms, because of interactions between barotropic (barotropic–barotropic term) and baroclinic (baroclinic–baroclinic term) eddies; similarly, $F_{\mathrm{BC}}(\gamma)$ is separated into the baroclinic–barotropic and baroclinic–baroclinic terms. Also, we calculated the spatial covariances between the resulting profiles and the zonally and temporally averaged barotropic (baroclinic) PV anomalies, normalized by their standard deviations. The resulting semicovariance is a measure of the efficiency and strength of the eddy forcing (or its components) in maintaining or resisting the jets. With all of this information, we examined how the eddy forcings of filtered eddies affect the jets, and the main results are discussed below and summarized in Tables 3 and 4.

Both barotropic–barotropic and baroclinic–baroclinic components of each barotropic-eddy forcing have similar magnitudes and structures; hence, their effects on the jets are similar. The only notable exception is LSLF eddies in the WB case, which have strong barotropic nature and exert mostly barotropic–barotropic-eddy forcing. The WME patterns, which are localized on westward jets, weakly resist the barotropic jets and strongly maintain the baroclinic jets. The corresponding baroclinic jets are maintained by the form stresses (i.e., negative isopycnal form drag) and weakly resisted by the Reynolds stresses. The EME patterns, which are localized on eastward jets, strongly maintain the barotropic jets and strongly resist the baroclinic jets. The corresponding baroclinic jets are maintained by the Reynolds stresses (i.e., negative viscosity effect) and strongly resisted by the form stresses.

The HFBM patterns, which are damped in the linear regime, are weakly localized on the east-/westward jets in the EB-/WB-flow regimes, except in the WB case with moderate γ. In the EB-flow regime, the HFBM patterns resist both the barotropic and baroclinic jets, and the baroclinic jets are resisted by both the Reynolds and form stresses. In the WB-flow regime, the eddy forcing of these modes is not correlated with the jets. The LSLFM patterns, in the EB-flow regimes, are localized mostly on the eastward jets, whereas in the WB-flow regime they are delocalized. These eddies maintain both barotropic and baroclinic components of the jets. The corresponding form stress is weak for small γ but relatively large for moderate γ. The SME patterns are localized on the eastward jets, and this constitutes a major difference from the underlying linear modes, which are localized on westward jets. Therefore, we conjecture that SME patterns are strongly nonlinear edge waves. We note that there is a temptation to use linear interpretation for describing SME because of the significant linear-spectrum "red power" in this part of k–ω space, but this interpretation cannot be correct. In the EB-flow regime, SME patterns maintain both the barotropic and baroclinic jets. For maintenance of the baroclinic jets, even weak west-/eastward drifts of these eddies correspond to the domination of the corresponding form/Reynolds stresses. In the WB-flow regime, SME patterns are dynamically neutral, except for the positive effect of form stress exerted by weakly westward-drifting component of SME. The FEM patterns are localized on eastward jets, and they maintain both barotropic and baroclinic components of the jets with Reynolds stresses.

The above analysis was extended to account for effects of eddy forcing on the LSLF eddies. The motivation here stems from the fact that the large-scale jet-like flow fluctuations (small k) are similar to the jets, and, therefore, can be similarly affected by the mesoscale eddies. We actually demonstrated this by calculating the instantaneous spatial correlations between the mesoscale eddy-forcing patterns and the time tendency of PV of the LSLF eddies and by averaging these correlations over time. The outcome is that all mesoscale eddy forcings have significant positive correlations with the LSLF eddies, and this is consistent with upscale energy transfers not only to the jets, but also to the transient jet-like flow features. We leave the complete analysis of the dynamics of these modes for the future.

We next examine the meridional correlations between eddies in the nonlinear regime, given that the linear analysis showed that most of the normal modes are localized on individual jets. In particular, there can be long-range meridional phase locking between the eddies

TABLE 3. Properties of large-Re eddies filtered in the k–ω spectral domain. Left column indicates quadrangles, and the other column corresponds to the EB- and WB-flow regimes with weak and medium values of the bottom friction coefficient. In each line there are 4 records: 1) abbreviation used for eddies in this quadrangle, 2) correlation between meridional profile of the eddy kinetic energy and zonally averaged zonal velocity and the word summarizing whether the eddies are correlated with the east- or westward jets, 3) semicovariance between the barotropic jets and the barotropic-eddy forcing and its decomposition into BT and BC Reynolds stresses, and 4) semicovariance between the BC jets and the BC-eddy forcing and its decomposition into the Reynolds R and form B stresses. Positive/negative values correspond to the eddy forcing (or its component) that maintains/destroys the jets. Units of the eddy forcing are $10^{-5} f_0^2$.

			EB, $\gamma = 0.1$		
		Jet	Correlation	Semicovariance (BT and BC)	Semicovariance (R and B)
1	WME	Westward	−0.56	$-0.14 = -0.07\text{BT} - 0.07\text{BC}$	$2.86 = -0.52R + 3.38B$
2	EME	Eastward	0.90	$3.45 = 1.25\text{BT} + 2.20\text{BC}$	$-6.38 = +18.72R - 25.10B$
3a	SME	Eastward	0.53	$1.17 = 0.88\text{BT} + 0.29\text{BC}$	$8.37 = 3.67R + 4.70B$
3b	SME	Eastward	0.83	$3.08 = 1.54\text{BT} + 1.54\text{BC}$	$14.97 = 15.19R - 0.22B$
4	HFBM	Eastward	0.39	$-0.51 = -0.37\text{BT} - 0.14\text{BC}$	$-3.08 = -2.35R - 0.73B$
5	FEM	Eastward	0.42	$0.37 = 0.22\text{BT} + 0.15\text{BC}$	$1.32 = 1.25R + 0.07B$
6	LSLFM	Eastward	0.35	$0.51 = 0.37\text{BT} + 0.14\text{BC}$	$1.76 = 1.39R + 0.37B$
			EB, $\gamma = 1$		
1	WME	Westward	−0.33	$-0.22 = -0.07\text{BT} - 0.15\text{BC}$	$2.94 = -0.51R + 3.45B$
2	SME	Eastward	0.67	$0.22 = 0.00\text{BT} + 0.22\text{BC}$	$3.08 = 1.47R + 1.61B$
3	EME	Eastward	0.89	$7.12 = 3.01\text{BT} + 4.11\text{BC}$	$-38.83 = 23.27R - 62.10B$
4	HFBM	Eastward	0.62	$-0.29 = -0.15\text{BT} - 0.14\text{BC}$	$-0.66 = -0.95R + 0.29B$
5	LSLFM	Eastward	0.64	$0.30 = 0.15\text{BT} + 0.15\text{BC}$	$6.53 = 1.69\text{R} + 4.84B$
			WB, $\gamma = 0.1$		
1	WME	Westward	−0.69	$0.07 = 0.00\text{BT} + 0.07\text{BC}$	$5.43 = -0.07R + 5.50B$
2	WME	Westward	−0.38	$0.00 = 0.00\text{BT} + 0.00\text{BC}$	$4.77 = 0.07R + 4.70B$
3a	SME	Eastward	0.31	$0.06 = 0.06\text{BT} + 0.00\text{BC}$	$3.74 = 0.29R + 3.45B$
3b	SME	Eastward	0.79	$0.15 = 0.00\text{BT} + 0.15\text{BC}$	$0.07 = 0.73R - 0.66B$
4	EME	Eastward	0.79	$1.10 = 0.73\text{BT} + 037\text{BC}$	$-4.77 = 0.44\text{R} - 5.21B$
5	HFBM	Westward	−0.42	$0.00 = 0.00\text{BT} + 0.00\text{BC}$	$0.07 = -0.15R + 0.22B$
6	LSLFM	Neither	0.22	$0.88 = 0.80\text{BT} + 0.08\text{BC}$	$1.03 = 0.29R + 0.74B$
			WB, $\gamma = 0.4$		
1	WME	Neither	0.03	$1.17 = 0.74\text{BT} + 0.43\text{BC}$	$19.89 = 0.81R + 10.08B$
2	EME	Eastward	0.66	$0.29 = 0.23\text{BT} + 0.06\text{BC}$	$-0.66 = 0.01R - 0.67B$
3	HFBM	Neither	0.01	$-0.06 = -0.06\text{BT} + 0.00\text{BC}$	$-0.28 = -0.14R - 0.14B$
4	LSLFM	Neither	0.18	$1.47 = 1.39\text{BT} + 0.00\text{BC}$	$3.38 = 0.59R + 2.79B$

localized on different jets, or, in the presence of weak jets, there can be significant power in the ''noodle'' mode characterized by a large meridional scale (Berloff et al. 2009). To examine these issues, we analyzed the meridional correlations of velocity streamfunction fluctuations in all eddy classes by calculating meridional autocorrelation functions $C_i(y, y_0)$, with respect to each reference latitude y_0 within the channel width ($0 < y_0 < L_y$). At each reference latitude, $C_i = 1$, but over some length scale it often decays to zero, and in between it can oscillate. We defined the corresponding meridional correlation length

$$L_i(y_0) = \int_0^{L_y} |C_i(y, y_0)|\, dy \tag{5}$$

and estimated it for all eddy classes, keeping in mind that a meridional length scale of typical jet is about $0.1L_y$, which is consistent with the fact that most of the linear normal modes are localized on the jets. We found that L_2 is slightly larger than L_1, but this difference is not significant. The shortest values of $L_i \approx 0.06 - 0.08L_y$ are found in flow regimes with large bottom friction (and weak jets), in all parts of k–ω spectra. In the solutions with weaker bottom friction (and strong jets), L_i is 1.5–2 times longer than in the strong bottom friction case, for all types of mesoscale eddies. However, the correlation length is always relatively long ($L_i \approx 0.2$–0.3) for the eddies with relatively small k (i.e., HFBM, LSLFM, and FEM); for example, for FEM, $C_i(y, y_0)$ does not decay to zero over the channel width, indicating that the signal is dominated by global channel modes. We also do not find significant differences in L_i between the large- and moderate-Re solutions, which is consistent with the fact that in both flow regimes most of the linear normal modes are localized on the jets.

TABLE 4. Properties of moderate-Re eddies filtered in the k–ω spectral domain. Layout and notations are as in Table 3.

			EB, $\gamma = 0.1$		
		Jet	Correlation	Semicovariance (BT and BC)	Semicovariance (R and B)
1	WME	Westward	−0.66	0.00 = 0.00BT + 0.00BC	$1.47 = 0.30R + 1.17B$
2	WME	Westward	−0.57	0.00 = 0.00BT + 0.00BC	$1.17 = 0.43R + 0.74B$
3	WME	Westward	−0.48	0.08 = 0.00BT + 0.08BC	$1.68 = 1.03R + 0.65B$
4	WME	Neither	0.06	0.00 = 0.00BT + 0.00BC	$0.74 = 0.59R + 0.15B$
5	EME	Eastward	0.40	0.37 = 0.07BT + 0.30BC	$0.14 = 2.94R - 2.80B$
6	EME	Eastward	0.69	0.95 = 0.66BT + 0.29BC	$-0.15 = 5.43R - 5.58B$
7	LSLFM	Neither	0.20	0.00 = 0.00BT + 0.00BC	$0.00 = -0.06R + 0.06B$
			EB, $\gamma = 1$		
1	WME	Westward	−0.43	0.88 = 0.58BT − 0.30BC	$3.38 = -1.83R + 5.21B$
2	EME	Eastward	0.72	12.84 = 5.65BT + 7.19BC	$-16.59 = 35.31R - 51.90B$
3	LSLFM	Eastward	0.42	0.51 = 0.30BT + 0.21BC	$4.26 = 1.46R + 2.80B$
			WB, $\gamma = 0.1$		
1	WME	Westward	−0.84	0.06 = 0.00BT + 0.06BC	$11.74 = -0.16R + 11.90B$
2	EME	Eastward	0.87	1.40 = 1.10BT + 0.30BC	$-3.74 = 0.22R - 3.96B$
3	LSLFM	Neither:	0.06	0.07 = 0.07BT + 0.00BC	$-0.22 = -0.07R - 0.15B$
			WB, $\gamma = 0.4$		
1	WME	Neither	−0.07	0.81 = 0.37BT + 0.44BC	$0.80 = -2.06R + 2.86B$
2	LSLFM	Neither	0.06	0.22 = 0.22BT + 0.00BC	$0.08 = -0.15R + 0.23B$

4. Conclusions and discussion

The main goal of this paper is to make further progress in understanding to what extent and how properties of the ocean's eddies are controlled by the underlying linear dynamics. To address this question, we spectrally analyzed solutions of an idealized, turbulent nonlinear model of mesoscale eddies generated by unstable, vertically sheared zonal flows at moderate and large Reynolds numbers. The central question that we ask is to what extent properties of eddies are controlled by the underlying linear dynamics? To answer this question, we took into account multiple alternating zonal jets generated and maintained by the eddies; these jets feed back on the eddies and alter the underlying linear properties. These linear properties are systematically analyzed in Part I of this paper. We concluded that many aspects of nonlinear eddies are consistent with the underlying linear dynamics and, therefore, can be understood in terms of linear normal modes. However, the linear modes are substantially modified by the large-scale background flow and alternating jets, and these effects are essential for the dynamics.

What are the general and fundamental reasons for such significance of the linear control in the strongly nonlinear flow regimes? One reason is the ''smearing'' effect of the potential vorticity inversion, which yields velocity field from distribution of PV anomalies. This inversion relationship averages out the small-scale structure of the PV anomaly field and, thus, projects eddies on relatively large-scale modes; and this paper quantifies to what extent these modes are similar to the underlying linear normal modes. The other reason is the existence of important long-range planetary waves (maintained by PV gradients) that strongly constrain flow fluctuations and, thus, slave them to become wave turbulence (Nazarenko 2011). Overall, the extreme point of view, that the linear dynamics is formally valid only for infinitesimal flow disturbances, and, therefore, is useless for describing finite-amplitude eddies, is overly pessimistic. Although a linear theory cannot predict amplitudes of the nonlinearly equilibrated eddies, in some flow regimes it can be used to predict structure and dispersion properties of not only the eddies but also the nonlinear eddy forcing. The linear-dynamics ability to predict some of these properties can be referred to as linear control over the nonlinear dynamics.

Solutions of our idealized dynamical model of anisotropic geostrophic turbulence are characterized by the presence of multiple alternating zonal jets that coexist and interact with transient wave-like eddies, as well as with isolated coherent vortices. We considered several typical flow regimes, at moderate (as in most of the previous studies) and large Re, with different degrees of latency of the jets, and with the large-scale background flow, which is either east- or westward. We focused on zonal wavenumber/temporal frequency spectra (i.e., k–ω spectra) because they conveniently demonstrate dispersion properties of zonally propagating transient eddies

and examined eddy patterns in different parts of the spectra. These properties were compared with the underlying linear normal-mode properties.

We focused primarily on the k–ω spectra but also considered more traditional wavenumber and frequency spectra. For each solution, we examined several eddy classes, corresponding to well-defined spectral regions. For each class, we focused on such important properties as horizontal and vertical structure and eddy forcing exerted on the underlying jets. First, we concluded that many aspects of the nonlinear eddies can be explained by the underlying linear dynamics. Second, we showed that the most unstable normal modes control a relatively small part of the spectrum, and most of the spectral power is contained in the nearly neutral, stable normal modes from other parts of the spectrum. In particular, there is a tendency of the nonlinear spectral power to populate a small-k and small-ω spectral region, and it is more pronounced at large Re. Third, we argued that in the presence of a weak background flow interpretation of eddies in terms of barotropic and baroclinic vertical modes is dynamically inconsistent because these modes are coupled by the linear dynamics; and we confirmed this coupling in the nonlinear solutions. Fourth, our analysis of the energetics suggests that the energy of the background flow enters mostly the parts of the spectrum controlled by the most unstable normal modes, and from there the energy is transferred to large-scale eddies and jets. Fifth, we found that a significant fraction of the eddies is localized in terms of the amplitude on either east- or westward jets; and estimates of the meridional coherency also confirm strong meridional localization of these eddies. Sixth, we found that the negative viscosity and negative isopycnal form drag effects associated with the eddy Reynolds and form stresses, respectively, are consistent with the underlying normal modes. Finally, we showed that spectral contribution of isolated coherent vortices, which are not significantly controlled by the linear dynamics, is modest.

Let us now discuss important differences between the approach taken in this paper and an approach based on local linear analysis, taken in some previous studies. In particular, an interesting attempt to compare nonlinear eddies from an eddy-resolving model of the Southern Ocean with local predictions of the underlying linear dynamics was made by Venaille et al. (2011). In this work the linear properties were defined in terms of the most unstable isotropic Fourier mode, which was calculated with respect to a horizontally uniform but vertically sheared background flow matching time-mean velocity at a given location. Our results imply that such a local approach should be applied with caution, because we demonstrated both the importance of meridional variations in the mean state (associated with jets) and the importance of slowly growing and damped linear modes in the nonlinear regime. Another implication of our results is to use great caution when applying the local approach for estimating eddy transfer properties and diffusivities (e.g., Green 1970; Killworth 1997; Smith and Marshall 2009; Tulloch et al. 2011; Eden 2011).

There are several limitations of our study, each suggesting further research avenues. First, our model did not include such important aspects as high baroclinic modes, more realistic three-dimensional background shears and density distributions, as well as topography and complex boundaries. Second, our work opened several important questions that could not be addressed within the limited scope of this paper: (i) the analysis and theory of long-lived coherent vortices (and, perhaps, nonlinear edge waves) on baroclinically unstable background shears, and (ii) the theory of the planetary wave turbulence, which would provide predictive understanding of nonlinear interactions between different normal modes. Encouraged by present results, we expect that wave turbulence can be a useful framework for more physically complex problems, but it may be easier to develop it, first, for the relatively simple problem explored here. Also, several research avenues can be undertaken to extend our spectral analysis. First, nonlinear solutions can be formally projected on the linear normal modes, and this will produce the corresponding spectral amplitudes and phases. The technical challenge here arises from the fact that the normal modes are not orthogonal in the meridional direction; therefore, some large-matrix manipulations will have to be involved. Second, from the above projection one can estimate triad interactions of the normal modes. Finally, we considered solutions with zonally uniform background PV, but, if this simplification is relaxed, the jets will tilt and drift (Boland et al. 2012), making the flow significantly more transient and changing its spectral properties.

Acknowledgments. PB acknowledges hospitality of the Department of Applied Mathematics and Theoretical Physics at the University of Cambridge, where most of this work has been done. Funding was also provided for PB by NSF Grant OCE 0845150, and for IK by NSF Grant OCE 0842834 and 1154923. Numerous discussions with Tom Farrar, as well as his help with spectral analysis, are graciously appreciated.

APPENDIX

Properties of Wavenumber, Isotropic Wavenumber, and Frequency Spectra

For each reference solution, we focused on potential vorticity anomalies and calculated double Fourier

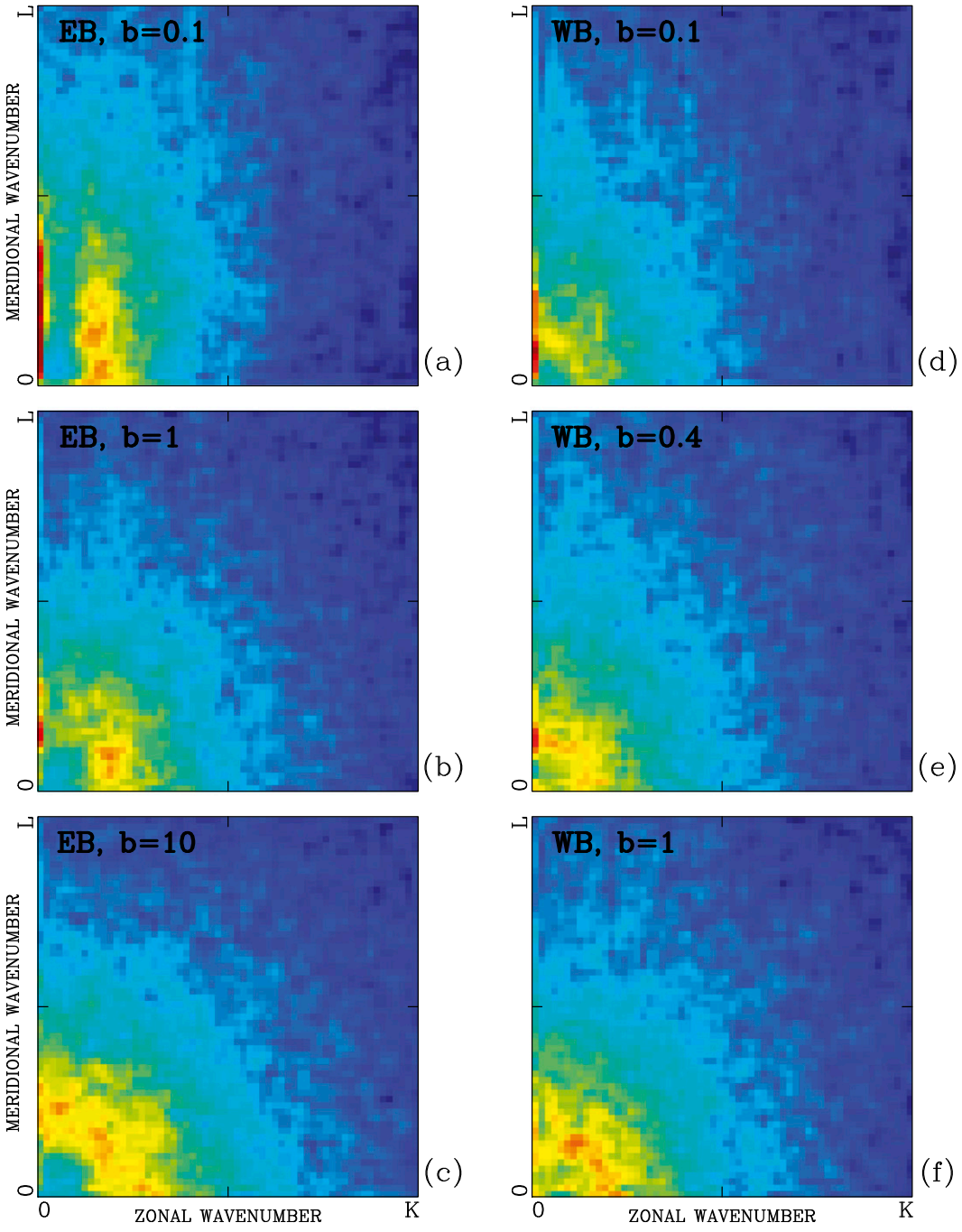

FIG. A1. Zonal/meridional wavenumber spectra of the reference solutions. Spectra of the large-Re instantaneous solutions for the EB/WB cases with (a),(d) weak; (b),(e) medium; and (c),(f) large bottom friction values. Plotted is $\log_{10}$ of the power of the PV anomaly, and the color scale is the same for all panels. Axis labels K and L are 1.7 (100 km period^{-1}). All four quadrants of the spectrum are added together, so that shown k and l are positive. Values of the high power for zero zonal wavenumbers correspond to the multiple zonal jets.

wavenumber spectra, referred to as k–l spectra (Fig. A1 shows these spectra for typical flow snapshots at large Re). There are several conclusions that can be made from visual inspection of these spectra. First, at lower values of bottom friction there is very strong condensation of spectral power at $k = 0$, that is, on the purely zonal Fourier modes. This spectral peak is still present at large γ, where the time-mean jets are absent—this indicates

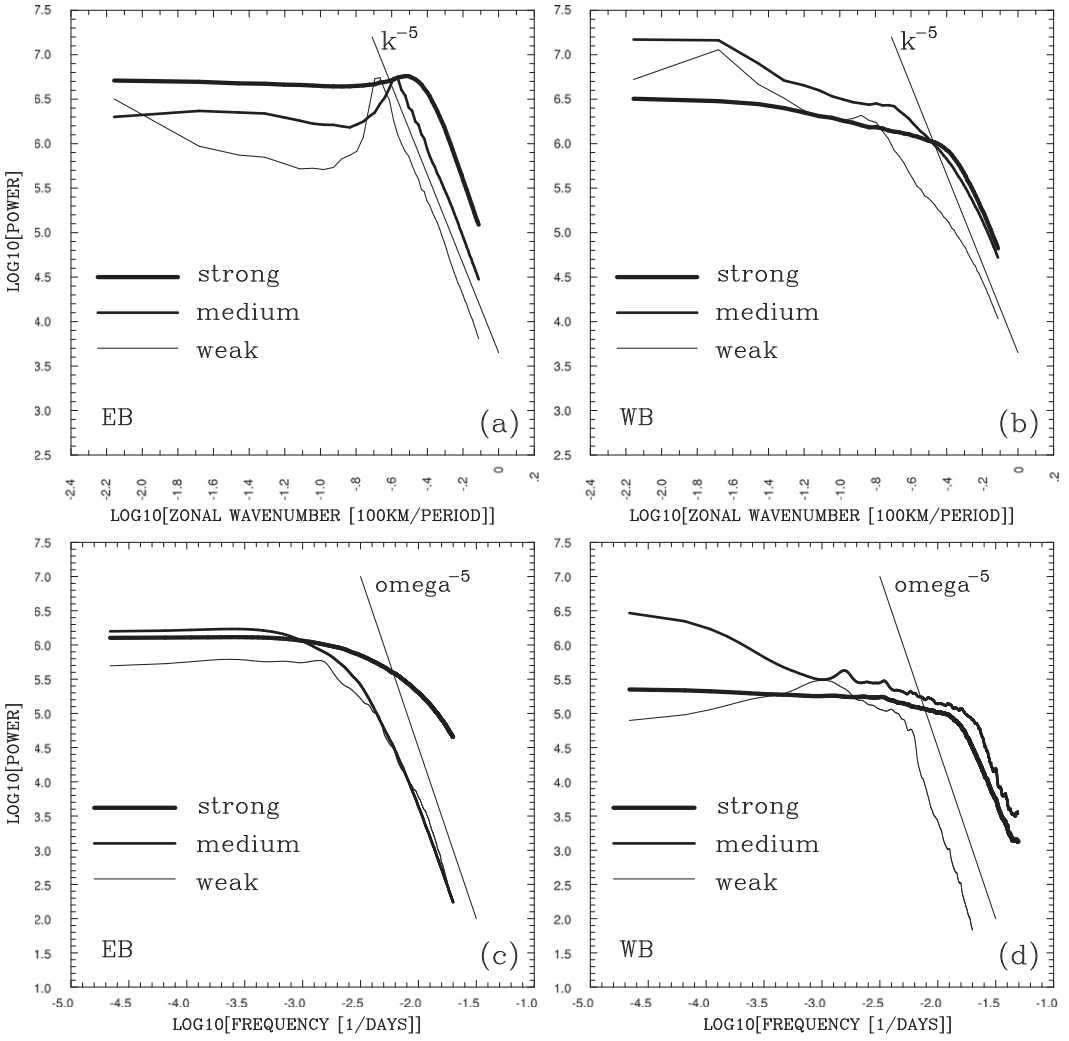

FIG. A2. (a),(b) Zonal-wavenumber and (c),(d) frequency spectra of the large-Re nonlinear solutions. EB- (left) and WB-flow regimes (right) are shown. Curves with different thicknesses correspond to the strong, medium, and weak bottom frictions. Line with slope −5 is shown for reference.

that transient jet-like modes (i.e., with very small k) are present in the solution—see I. Kamenkovich et al. (2013, unpublished manuscript) for discussion of this feature. The power at $k = 0$ is distributed over many zonal modes with different meridional scales, more so in the strong-jet-flow regime at small values of γ. This is because although the jets are meridionally nearly periodic, they are not purely sinusoidal. Second, in all flow regimes there is a distinct ''mesoscale'' spectral maximum. When the jets are strong, this maximum is noticeably anisotropic, in the sense that, for relatively narrow range of k values, there is relatively broad range of l values—this is an indication that many eddies are meridionally localized on individual jets.

In an attempt to find some spectral universality of more simple spectra, we calculated time-mean isotropic-wavenumber and frequency spectra (Fig. A2). The main features of the isotropic spectra are the following. At low wavenumbers the spectra are either flat or slightly red; at mesoscale wavenumbers all spectra, except for the large-Re WB case, have significant ''bump'' of power, which is larger in the regimes with more pronounced jets; and at high wavenumbers there are rather steep spectral tails, but no universality in their slopes. At large Re locations of the mesoscale-wavenumber ''bumps'' depend on γ, so that smaller values of γ result in the noticeably smaller k; but at moderate Re location of the ''bumps'' is insensitive to γ. The frequency spectra look similar: steep decays of the power at high frequencies, flat power at low frequencies, and no maximum at mesoscale frequencies. To summarize, both isotropic wavenumber and frequency spectra exhibit no universal shapes and strongly depend on the background flow and Re.

REFERENCES

Berloff, P., and I. Kamenkovich, 2013: On spectral analysis of mesoscale eddies. Part I: Linear analysis. *J. Phys. Oceanogr.,* **43,** 2505–2527.

——, ——, and J. Pedlosky, 2009: A mechanism of formation of multiple zonal jets in the oceans. *J. Fluid Mech.,* **628,** 395–425.

Boland, E., A. Thompson, E. Shuckburgh, and P. Haynes, 2012: The formation of nonzonal jets over sloped topography. *J. Phys. Oceanogr.,* **42,** 1635–1651.

Early, J., R. Samelson, and D. Chelton, 2011: The evolution and propagation of quasigeostrophic ocean eddies. *J. Phys. Oceanogr.,* **41,** 1535–1555.

Eden, C., 2011: A closure for mesoscale eddy fluxes based on linear instability theory. *Ocean Modell.,* **39,** 362–369.

Galperin, B., S. Sukoriansky, and N. Dikovskaya, 2010: Geophysical flows with anisotropic turbulence and dispersive waves: Flows with a beta-effect. *Ocean Dyn.,* **60,** 427–441.

Green, J., 1970: Transfer properties of the large-scale eddies and the general circulation of the atmosphere. *Quart. J. Roy. Meteor. Soc.,* **96,** 157–185.

Killworth, P., 1997: On the parameterization of eddy transfer. Part I: Theory. *J. Mar. Res.,* **55,** 1171–1197.

Nazarenko, S., 2011: *Wave Turbulence.* Springer, 295 pp.

Smith, K., and J. Marshall, 2009: Evidence for enhanced eddy mixing at middepth in the Southern Ocean. *J. Phys. Oceanogr.,* **39,** 50–69.

Tulloch, R., J. Marshall, C. Hill, and K. Smith, 2011: Scales, growth rates, and spectral fluxes of baroclinic instability in the ocean. *J. Phys. Oceanogr.,* **41,** 1057–1076.

Vallis, G., and M. Maltrud, 1993: Generation of mean flows and jets on a beta plane and over topography. *J. Phys. Oceanogr.,* **23,** 1346–1362.

Venaille, A., G. Vallis, and S. Smith, 2011: Baroclinic turbulence in the ocean: Analysis with primitive equation and quasigeostrophic simulations. *J. Phys. Oceanogr.,* **41,** 1605–1623.